New Collider Detectors and Physics Capabilities

IMPROVEMENT PROGRAMME OF THE UA2 DETECTOR

The UA2 Collaboration

Bern - Cambridge - CERN - Milan - Orsay (LAL)
Pavia - Pisa - Saclay

Presented by Jean-Marc GAILLARD
Laboratoire de l'Accélérateur Linéaire
91405 Orsay , France.

1. INTRODUCTION

The UA2 experiment took its first data in November 1981 and has been operating smoothly since then. The very successful performance of the $Sp\bar{p}S$ collider has given us the opportunity to collect a large amount of very fruitful data [1-7].

After a long shut-down in 1986, the $Sp\bar{p}S$ collider will resume operation with a substantially higher luminosity than presently available. The recently approved Antiproton Collector (ACOL) should allow for a total integrated luminosity of nearly 10 pb^{-1} by the end of 1989. In order to make the best use of the increased luminosity in terms of physics results the performance of the present UA2 detector has to be simultaneously improved.

The emphasis placed in the present design [8,9,10,11] on high mass final states containing parton jets, electrons and neutrinos has proven to be an excellent choice, mostly because of the low transverse momentum usually given to spectator particles (not directly involved in the short distance collision of interest). As a result of the high quality of the UA2 calorimetry (fine segmentation, tower geometry) we were able to give the first evidence for jet production at the Collider and for a resolved $Z^0 \to e^+e^-\gamma$ decay. The absence of magnetic field in the central region turned out to be a good choice since it does not significantly deteriorate the electron identification power as soon as the electron transverse momentum exceeds ≃ 25 GeV/c and does not preclude competitive performance on the major physics issues. Similarly, the lack of muon detection, dictated by the desire to avoid the use of bulky equipment, such as thick absorbers and large magnetic field volumes, does not substantially impair the physics output of the UA2 detector. It is true that the restriction of lepton detection to electrons and neutrinos precludes their observation amid jet fragments, while significantly better results might be achieved with muons.

We do not propose, therefore, to alter the major design options of the present UA2 detector but rather to improve its performance in the domains where it is already effective : the detection of electrons, neutrinos and hadron jets.

The importance of a good missing transverse energy detection capability was not fully recognised when UA2 was designed in 1978. It now appears essential, not only to study final states containing an electron-neutrino pair, but also to search for possible supersymmetric particles, ultimately expected to decay into undetected photinos. Dead regions, such as the magnet coils of the forward UA2 spectrometers, and the lack of coverage below 20°, preclude an accurate missing transverse energy measurement. For example a two-jet event having a mass of ≃ 50 GeV/c^2 is detected as a single jet event in ≃ 2% of the cases, the other jet escaping detection.

The solid angle over which a hermetic coverage is necessary depends upon the mass range to be explored : a Monte Carlo study indicates that a coverage down to ≃ 10° from the beam line should be adequate. We propose therefore to extend down to this angle the transverse energy flow measurement presently performed in the central calorimeter, by replacing the forward spectrometers with segmented calorimeter end caps. In doing so we shall lose the ability to measure particle charges in this region but we consider the gain of improving on neutrino detection to be more important.

The early discoveries of the $W^{\pm}$ and Z^0 bosons through their $e\nu$ and e^+e^- decay modes illustrate well the power of electron identification as a mean of selecting interesting events among the bulk of hadronic collisions. In the present UA2 detector, jets can fake electrons at a level of the order of 10^{-5} of the inclusive jet yield. While this background is much lower than the electron signal from W and Z^0 decays, it is higher than the expected signal from semileptonic decays of t-quarks (m(t) < 40 GeV) by about one order of magnitude. An improvement over the present situation implies a simultaneous discrimination against the two major types of misidentified electrons : converted photons from π^0 decays and unresolved π^0-$\pi^{\pm}$ pairs.

2. CALORIMETER END CAPS

In order to implement the transverse energy flow measurement down to small angles we propose to replace the present forward spectrometers with segmented calorimeter end caps. This approximately triples the longitudinal phase space coverage of the present central calorimeter and improves accordingly the ability of our apparatus to detect hadron jets and to provide an accurate measurement of missing transverse energy. The design provides for electron identification down to $\simeq 20°$ with a rejection power against background similar to that achieved in the central region.

We have studied the expected performance in relation to the measurement of transverse energy by simulating with a Monte Carlo programme the response of the detector to a set of two-jet events generated with ISAJET [12]. The detector coverage extends over a range of polar angles between θ_m and $180° - \theta_m$. Figure 1 shows the dependence upon θ_m of the average missing transverse energy under the assumption that one of the two jets has $p_\perp^{jet} > 25$ GeV/c and $20° < \theta_{jet} < 160°$. Figure 2 shows the distribution of the fraction of events having a missing transverse energy in excess of 20 GeV, f_{20}. A contribution of $\simeq 10^{-3}$, from events containing semi leptonic decays of heavy flavours, remains in the case of an "ideal" detector ($\theta_m = 0$, no energy measurement errors but no muon nor neutrino detection). For a realistic detector f_{20} levels off at $\simeq 10^{-2}$ for any $\theta_m < 10°$, one order of magnitude lower than in the present design. The results shown in fig.1 and 2 are illustrative of the performance expected in the kinematical domain of practical interest and suggest to extend the end cap coverage down to $\theta_m \simeq 10°$. This implies the instrumentation of the forward cones down to $\theta_m \simeq 5°$ to allow for a reasonable margin around the actual fiducial volume.

The general layout is illustrated in fig.3. The calorimeter end caps are shown without their movable support structure which will allow recessing the calorimeters from the beam pipe during machine developments with high radiation levels.

Each end cap is divided into sectors subtending $\Delta\phi = 30^\circ$ in azimuth. The absorber plates in each sector are continuous over the whole polar angle region $5.6^\circ < \theta < 45^\circ$, the segmentation into cells (towers) is defined by the scintillator plates. The wavelength shifter (WLS) plates collect the light of each cell at about constant azimuth with a segmentation of $\Delta\phi = 15^\circ$ for $\theta > 12.7^\circ$ and $\Delta\phi = 30^\circ$ for $\theta < 12.7^\circ$. Each tower consists of an electromagnetic and an hadronic calorimeter compartments. For both compartments the readout will be made by WLS plates on opposite sides of each cell. The light is channeled via a twisted strip light guide optics onto Philips XP2012 B photomultipliers.

The parameters of the end cap calorimeter are given in table 1.

3. UPGRADED VERTEX DETECTOR

3.1 Introduction

Moving outwards from the interaction region the main components of the new design include (figure 4)

i) A small diameter beryllium vacuum chamber to be installed in 1985,

ii) A jet chamber vertex detector (JVD) providing an accurate measurement of the longitudinal and transverse positions of the event vertex,

iii) A matrix of silicon counters with the double purpose of measuring ionisation and helping in pattern recognition,

iv) A pair of transition radiation detectors (TRD) providing an additional rejection factor of at least an order of magnitude against fake electrons,

v) A multilayer scintillating fibre detector (SFD) for tracking and for measuring early electromagnetic showers developing after a 1.5 radiation length thick converter.

The new design is expected to substantially reduce the two most significant sources of backgrounds faking electrons: converted photons from π^0 decays and narrow π^0-charged hadron pairs (overlaps).

The insertion of a transition radiation detector, a key feature of the new design, is at the price of dedicating to it a major fraction of the space available in the central region of UA2 (about half of the radial range). In turn this implies very efficient and compact tracking devices fitting in the remaining available space: the JVD and silicon array in the inner region, the SFD in the outer region. Both have the ability to measure track segments. In addition the outer cathodes of the TRD chambers are equipped with strips to help match the two regions.

While inner tracking provides direct localisation in space (charge division on the JVD wires and silicon pads), the SFD measures three stereoscopic projections. The stereo angle has been chosen small enough to reduce ghost tracks to a satisfactory level while retaining sufficient localisation accuracy. The outer layers of the SFD act as a preshower counter, thus providing a compact and unified design in the angular range covered by the central UA2 calorimeter. Modifications to the design of the extreme electromagnetic calorimeter cells have been necessary to enlarge the space available for the UA2 central detector.

The overall dimensions of the UA2 central detector have been defined to match the geometry of the central and end cap calorimeters and to provide tracking capability over the solid angle in which electrons are to be identified. This implies complete coverage in azimuth (Φ) and a polar angle (θ) coverage from 25° to 155° allowing for vertex excursions of ±200 mm along the beam direction (z). This latter constraint is forced on us by the geometry of the central calorimeter. While it is perfectly adequate in the present mode of Collider operation it would become too small if longer bunches were used as the result of a modification of the RF system.

The UA2 central detector will be supported from the central calorimeter and the various cables (≅600 cm^2 in cross-section) connected to its end plates are channelled to the UA2 cable-rails through the space between the central and end-cap calorimeters.

3.2 Jet Chamber Vertex Detector (JVD)

The design of the JVD, constrained to fit between the vacuum pipe ($R = 32$ mm) and the silicon array ($R = 140$ mm), is of the jet chamber type in order to satisfy the following requirements:

i) to measure space points in order to minimize ambiguities in the event reconstruction;

ii) to sample at least 12 space points per track with ≤ 150 μm accuracy in $R \times \Phi$;

iii) to separate nearby tracks in projection: $R \times \Delta\Phi \leq 1$ mm ;

iv) to provide good accuracy in z, both to separate double vertices and to allow precise extrapolation to the outer tracking devices;

v) to minimize photon conversions, implying a good transparency.

Longitudinal and transverse cross-sections are shown in fig.5. The detector has an outer radius of 135 mm, an inner radius of 35 mm, and a total length of 1600 mm (excluding the electronics). The chamber is divided into 16 azimuthal sectors, each equipped with 13 (staggered) sense wires 1100 mm long at 6.5 mm spacing, with guard wires interspersed among them (fig.5). Tracks will be measured down to $\theta = 25°$, with allowance for ± 200 mm excursions of the vertex along the beam. To minimize the material between the beam and the sensitive region, only the external cylindrical wall will carry the mechanical tension of the wires. Digitization of the drift time and readout of the z coordinate by charge division will be provided by the 100 MHz Flash-ADC (FADC) system developed at CERN by F. Bourgeois [13]. To enhance two-track separation capability we plan to operate the chamber with a "slow" gas (90% CO_2 + 10% Isobutane), at a drift velocity $\approx$ 1cm/μs (E/P = 1.3 kV/cm/atm).

To improve the accuracy of the track extrapolation to the SFD (R $\cong$ 400 mm), a cathode readout of the outermost sense wires using 168 cylindrical strips perpendicular to the beam direction measures the z-coordinate of the avalanches on every sense wire .

3.3 Silicon Array

On a cylinder of radius 140 mm around the beam pipe, we intend to construct a matrix of 432 silicon counters, each divided into seven individual readout channels (3024 in total). This array is immediately outside the JVD. It will be used in conjunction with that detector to:

i) reject photon conversions by providing, with good granularity, a measurement of the ionisation of charged tracks, and

ii) help track reconstruction by providing a space-point measurement.

It is intended to install this array before the 1985 data taking period and it has therefore been designed to be also compatible with the existing vertex detector.

Each silicon counter has a size of 61 × 40 × 0.3 mm^3. Nine counters are arranged on each of 48 fibreglass boards. Each board covers an azimuthal interval of 15° and half the polar angle range. By overlapping individual counters on the board the array has a negligible inactive area. On each board low noise amplifiers are mounted behind the detectors, and the signals are subsequently transferred to the end of the detector via a multi-layer circuit board. Shaping amplifiers, track-and-hold circuits and multiplexing electronics are mounted at the end of each board. Each board is enclosed in a box and mounted on a thin support cylinder.

Twelve prototype counters, of the final design specification [14], have been extensively tested, and the prototype tests are continuing. Tests which are underway include:

i) long-term leakage current tests,

ii) tests of pulse-height resolution using a Ru^{106} β-source,

iii) the dependence of the above on the applied bias voltage,

iv) radiation damage, including tests with a 1mCi Sr^{90} source, and with radiation in the SPS tunnel.

Within the limited statistics of present radiation damage tests, the counter deterioration (measured as an increase in leakage current) is ≅ 1 nA/cm^2/Gray in the UA2 environment; this suggests, for the present counter design, a maximum tolerable dose of ≅ 200 Gray. No problem is therefore expected, apart from possible accidental beam losses (the total dose during the 1983 running period was ≤ 3 Gray at the proposed array location).

Typical pulse-height spectra for counters passing our design criteria are shown in fig.6. A rejection factor against photon conversions of 15 to 20, with 90% efficiency, is expected.

3.4 Transition Radiation Detector (TRD)

The TRD is inserted in the 210 mm of radial space between the silicon array and the SFD. It is made of two modules, each consisting of a lithium radiator to emit X-rays and a xenon proportional chamber to detect them.

Each radiator is cylindrical and has a thickness of 80 mm. It contains a stack of 400 lithium foils, 40 μm thick , separated by 160 μm. The spacing is maintained by corrugations in the foils. The total lithium weight is 50 kg. The average number of photons produced by an electron of energy > 5 GeV traversing the radiator at normal incidence and subsequently absorbed in the xenon chamber is 2. Their average energy is 6 keV.

The xenon chambers consist of two layers of gas, 10 and 6 mm thick, separated by a grid of wires connected to ground. The gas mixture is 70% xenon, 30% CO_2. In the first layer, a drift velocity of 20 μm/ns is obtained with an electric field of 400 V/cm. The second layer is used as an amplification stage. The signal wires are separated by 4.4 mm and interspersed with field wires (fig.7). The signal wires are at a voltage of 1.6 kV and the two cathodes of the amplification stage are grounded. This allows the outer cathode to be made of helical strips from which the charge can be read out.

Each module is about 0.015 thick in both radiation length and interaction length.

The wires are connected to preamplifiers and the signals are measured in a 100 MHz FADC [13]. The strips are connected to preamplifiers and the integral of the charge induced by the avalanche is measured in ADC's. Since the signals coming from the drift space and the amplification stage arrive at different times, we plan to measure them independently.

We have used a computer programme [15] to evaluate the electron detection efficiency and the rejection against hadrons, and to optimize the radiator and chamber parameters. The results of this programme have been compared to real test measurements. They show that a two-module design is more efficient than a single-module design given the available space. Using the cluster counting method, we expect a rejection of a factor 15 against hadrons with an efficiency of 80% for electrons. This performance improves by a factor 3 when the polar angle of the electron changes from 90° to 30°. The rejection is of course degraded when two ionizing particles hit the same wire but the measurement of the charge induced on the strip will help to recover part of this loss.

3.5 Scintillating Fibre Detector (SFD)

Recent developments in scintillating plastic fibres made at Saclay offer an attractive possibility to construct a compact position detector with good track reconstruction efficiency and adequate spatial accuracy. As emphasized above compactness is absolutely necessary to provide space within the UA2 apparatus for the TRD. The present design of the SFD is based upon:

i) extensive tests that we have made with fibres during the second half of 1984,

ii) Monte Carlo studies of the track reconstruction properties using simulated $p\bar{p}$ events,

iii) measurements on, and investigations of, the various components (image intensifiers, CCD, digitizers) necessary to read and digitize the fibre information.

The SFD whose general layout is shown in fig.6, has a radial thickness of 60 mm at an average radius of 410 mm. It consists of about 60000 fibres, with a total length of 150 km, arranged in seven groups of three layers (triplets). In each triplet, the angles of the fibres with respect to the beam axis are $-\alpha$, 0, and α for the three layers respectively. This provides space coordinates from three stereoscopic projections. Within the angular range covered by the central UA2 calorimeter, a converter (1 and 0.5 radiation lengths respectively) is inserted in front of each of the two outer triplets, which are thus used as a preshower counter.

The choices for the design of the detector are based on the standard fibres which we have tested . They are made of a core of polystyrene, doped with POPOP and butyl-PBD, with a thin cladding ($\cong$10 μm) and have a numerical aperture of 0.62. These fibres are currently produced by Saclay (STIPE) in lengths of 600 m with a 1 mm diameter.

We plan to view the fibres from one end only and to place a reflector at the other end. We expect on average 91% efficiency per fibre for particles at $\theta = 90°$. For other values of θ the average efficiency becomes closer to 100%.

A schematic representation of the read_out system is shown in fig.8. It is composed of three parts. The light output from the fibres is amplified with a photon gain of 10^4 by the image intensifiers (II). The light is then converted by a charge coupled device (CCD) into a signal which is read by the digitizer and stored in a memory. The photon gain of the II system is chosen such that the average signal per CCD element (pixel), within the area corresponding to a fibre hit by a charged particle, is ten times larger than the noise level of the CCD. The principle of operation is also indicated in fig.8. The gate of the II system is normally open and information accumulates in the CCD. About 1 μs after each crossing an external trigger decision (not using the fibre information) leads to one of the two following sequences:

i) no-trigger case: a fast-clear pulse is applied to the CCD, draining away the accumulated charge in ≤ 1.5 μs. The II gate stays open and new information is collected in the CCD.

ii) trigger case: the gate on the II system is closed to prevent illumination from subsequent $p\bar{p}$ interactions while reading the CCD information related to the event associated with the trigger (≅4 ms). When the CCD reading is completed the II gate is reopened.

From investigations with several firms, it has become clear that three amplifying stages are necessary to meet our gain specifications: a moderate gain unit , a high gain II tube with microchannel plate, an other moderate gain unit . The first and the third units are demagnifying the fibers image.

The fibre optic window at the exit of the II chain is directly coupled to a CCD where the light is converted to electrical charges which are stored. It is essential that unwanted information can be cleared off from the device during the time available between two $p\bar{p}$ crossings. This can be achieved by using the antiblooming system with which some commercial CCD's are equipped. In collaboration with the manufacturer [16], we have tested the CCD TH7852 which we plan to use, and we have found that it can be fast-cleared by applying a pulse of ≤ 1.5 μs duration to the antiblooming input.

The CCD TH7852 has an optical area of 5.8 × 4.3 mm^2 with 144 × 208 sensitive elements (pixels). Each pixel has an active area of 19 × 30 μm^2 and a geometrical area of 28 × 30 μm^2. With the demagnification of the II chain , a 1 mm diameter fibre may illuminate up to about 20 pixels.

For events satisfying the trigger requirement, the content of each CCD is read out. We consider that pulse height information is useful in pattern recognition, and necessary for the preshower part of the SFD. In addition, since in a typical event particle tracks cross ≅ 2% of the fibres, the compaction of data is essential for an efficient and economical utilization of memory.

4. END CAP TRACKING AND PRESHOWER

The compactness of the upgraded UA2 apparatus constrains the tracking and preshower devices to be confined in a small volume inside the central calorimeters.

Taking into account the accuracy required to localize the shower, it turns out that the choice of proportional tubes with a 1 cm wire spacing, using extruded aluminium profiles allows for compactness and easy large-scale production. A proportional mode of operation is chosen for both devices in order to cope with high particle densities which could be expected from the higher luminosity at the collider and the absence of magnetic field, as well as maintaining the widest possible dynamic range for measuring the total particle multiplicity in electromagnetic showers. In addition analog measurements allow for better space localization of the electromagnetic shower by determining the center of gravity of the charge collected in each plane of the detector.

Stacks of three planes of tubes with a cross-section of 9 × 9 mm^2, at 0°, $\pm 67.5^\circ$ stereo-angle, are used as modular elements. Sectors covering 45° in azimuth are the best compromise between dead space and total number of electronic channels (about 11500). Adjacent sectors are chosen in place of a staggered geometry since with the construction technique considered the frame dimensions can be minimized and the advantage of a uniform small distance between preshowers and calorimeters largely compensates for the small losses in sensitive area (≅ 8%)

Each sector consists of two stacks (each with three planes) for the tracking part to localize the track impact point, followed by a radiator and another stack of three planes to detect and localize the electromagnetic showers. The radiator built as an iron-lead sandwich 1.5 r.l. thick, is the supporting element of the entire chamber structure, thus allowing for a uniform transparency over the full azimuth. The preshower chambers will be equipped with multiplexed analog readout.

The performance of a set of aluminium proportional tubes of the type described above was studied using hadron and electron beams at the SPS. The detector efficiencies for electrons and hadrons are shown in figure 9 as a function of the cut on the pulse height distributions for various experimental conditions, and the correlation between the two efficiencies at 10 and 40 GeV/c.

The space resolution can be evaluated from the distribution of the residuals between the detected charge centroid and the beam impact coordinates. The resulting resolution is about 3 mm on each coordinate plane for non-showering particle tracks and 2.3 mm for the shower charge centroid. An extrapolation to a multiple-plane structure yields a space resolution of less than 2 mm for the actual detector.

5. CONCLUSIONS

We are in the process of modifying the present UA2 detector with the aim to match its performance to that of the improved S$\bar{p}$pS Collider.

The new design results from a number of choices dictated by the following considerations:

i) The upgraded UA2 must be operational in 1987, as soon as the Collider resumes operation, in order to maximise its physics output during the period when TEV 1, with nearly three times as high a c.m. energy, has not yet taken over leadership.

ii) The upgraded UA2 must remain competitive on the major physics issues rather than diversify its detection capabilities.

iii) Priority is given to the quality of the missing transverse energy measurement.

iv) Modifications to the vertex detector aim at ensuring that multivertex events can be reconstructed and at improving the detector performance in relation with electron identification.

REFERENCES

1. M. Banner et al., Phys. Lett. 118B (1982) 203.
2. P. Bagnaia et al., CERN-EP/84-12.
3. P. Bagnaia et al., Z. Phys. C 20 (1983) 117.
4. UA2 Collaboration, CERN 83-04 (1983), p. 190.
5. M. Banner et al., Phys. Lett. 122B (1983) 476.
6. P. Bagnaia et al., CERN-EP/84-39
7. P. Bagnaia et al., Phys. Lett. 129B (1983) 130.
8. A. Beer et al., CERN-EP/83-175 , A. Beer et al., Nucl. Inst. Meth. 224 (1984) 360.
9. M. Dialinas et al., LAL-RT/83-14.
10. C. Conta et al., CERN-EP/83-176.
11. K. Borer et al., CERN-EP/83-177.
12. F.E. Paige and S.D. Protopescu, BNL-31987.
13. F. Bourgeois, Nucl.Inst.Meth. 219 (1984) 153, F. Bourgeois et al., CERN/EF 84-14, Oct 1984.
14. Micron Semiconductor Ltd, Lancing,Sussex,United Kingdom.
15. Courtesy of B.Dolgoshein and I.Gavrilenko; see also NA32 proposal.
16. Thomson-CSF, CCD TH7852.

TABLE 1 : End Cap Calorimeter Parameters

Electromagnetic calorimeter	
technique	Pb-scintillator sandwich K-27 wavelength shifter read out
material	32 Pb plates, 3 mm thick 33 scintillator plates, 4 mm thick (Polivar)
sampling	0.54 to 0.70 X_0
total thickness	17.1 to 24.4 X_0
Hadronic calorimeter	
technique	Fe-scintillator sandwich K-27 wavelenght shifter read out
material	Fe plates, 25 mm thick scintillator plates, 4 mm thick (Polivar) $5^\circ < \theta < 20^\circ$: 38 plates $20^\circ < \theta < 40^\circ$: decreasing from 38 to 29 plates
sampling	0.15 to 0.19 λ_0
total thickness	5.6 to 6.2 λ_0 (0.6 to 0.8 λ_0 in addition from the electromagnetic calorimeter)
Segmentation	
structure	towers pointing to the centre of the detector
cell size	$1.0 < \lvert\eta\rvert < 2.2$: $\Delta\phi \times \Delta\eta = 15^\circ \times 0.2$ $2.2 < \lvert\eta\rvert < 2.5$: $\Delta\phi \times \Delta\eta = 30^\circ \times 0.3$ $2.5 < \lvert\eta\rvert < 3.0$: $\Delta\phi \times \Delta\eta = 30^\circ \times 0.5$ (only hadronic)
depth segmentation	one electromagnetic and one hadronic compartment
sector	30° in azimuth, 24 sectors in total rotation angle 50 mrad (see text)
number of cells	electromagnetic 312 hadronic 384
number of channels	2 PM's per cell, 1392 total
Approximate weight	
	120t for each end cap

The thicknesses in radiation length (X_0) and absorption length (λ_0) vary as a function of the polar angle θ between 5° and 40° with respect to the beam axis.

FIGURE CAPTIONS

Figure 1 : Average missing transverse energy as a function of θ : a) "ideal" detector, b) new UA2 calorimeter, c) present UA2 set-up.

Figure 2 : Fraction of events with a missing transverse energy in excess of 20 Gev as a function of calorimeter coverage for the same event sample as in fig.1 and for the same cases a),b),c) .

Figure 3 : General layout of the end cap calorimeters. The movable support structures which will allow to recess the end caps from the beam pipe are not shown.

Figure 4 : The new central detector: schematic layout,longitudinal view.

Figure 5 : The JVD : a)longitudinal view, b)transverse cross-section, c) layout of a cell . 1:beryllium pipe, 2: pressure vessel, 3: outer chamber wall, 4: inner chamber wall, 5: end plate for wire support, 6: signal and HV feed-throughs .

Figure 6 : Pulse spectra of a silicon prototype detector : bias voltage of -60 V,Ru ^{106} source, resolutions given in percent of minimum ionizing particle response, resolution of signal peak evaluated from half width at half maximum. Pedestal widths are measured in percent of the peak pulse-heights

Figure 7 : Cross section of the inner TRD module showing the lithium radiator and the xenon chamber.

Figure 8 : Principle of operation of the readout and digitization system of the SFD.

Figure 9 : End cap preshower : a) Electron efficiency as a function of the m.i.p. cut, b) Hadron efficiency vs m.i.p. cut, c) Hadron efficiency as a function of the electron efficiency for various electron momenta and converter thicknesses.

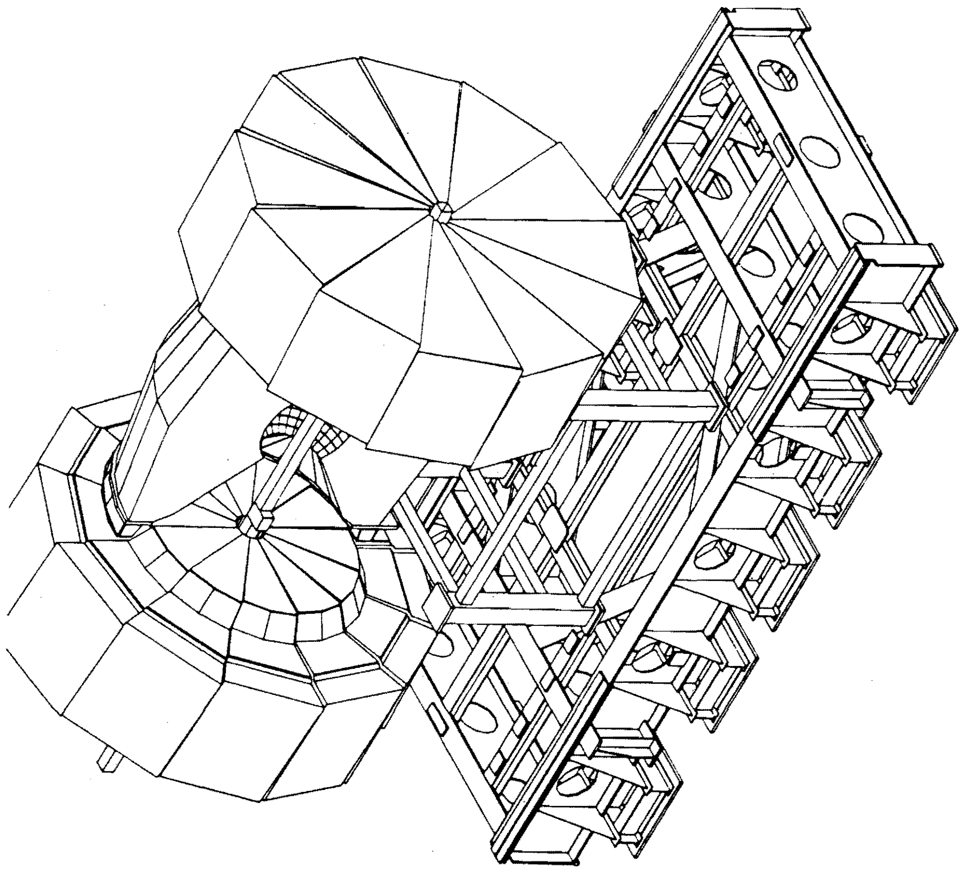

Fig. 3

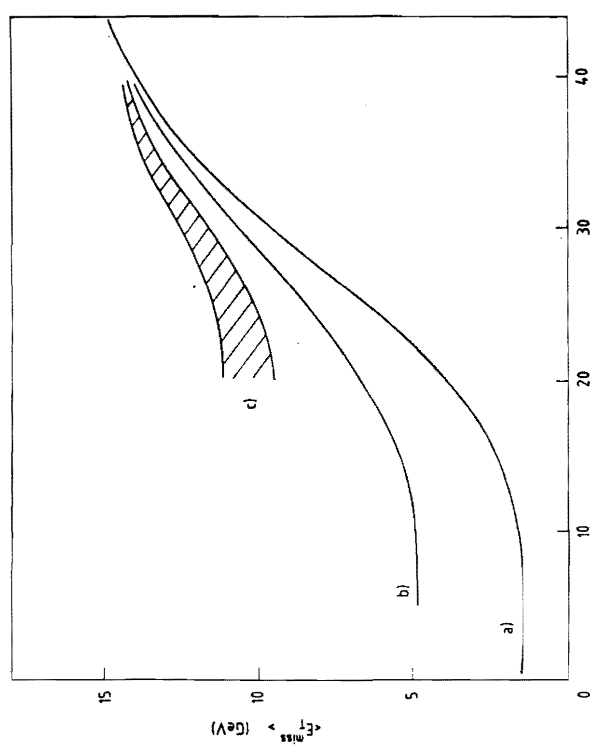

Fig. 1

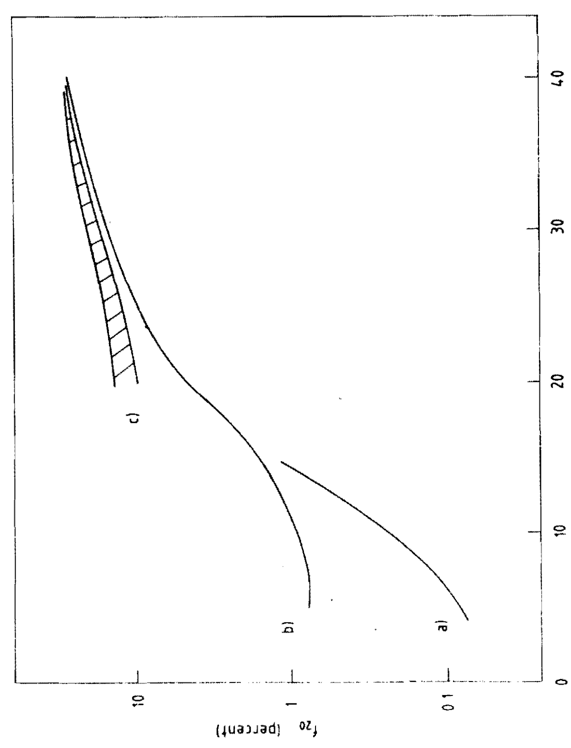

Fig. 2

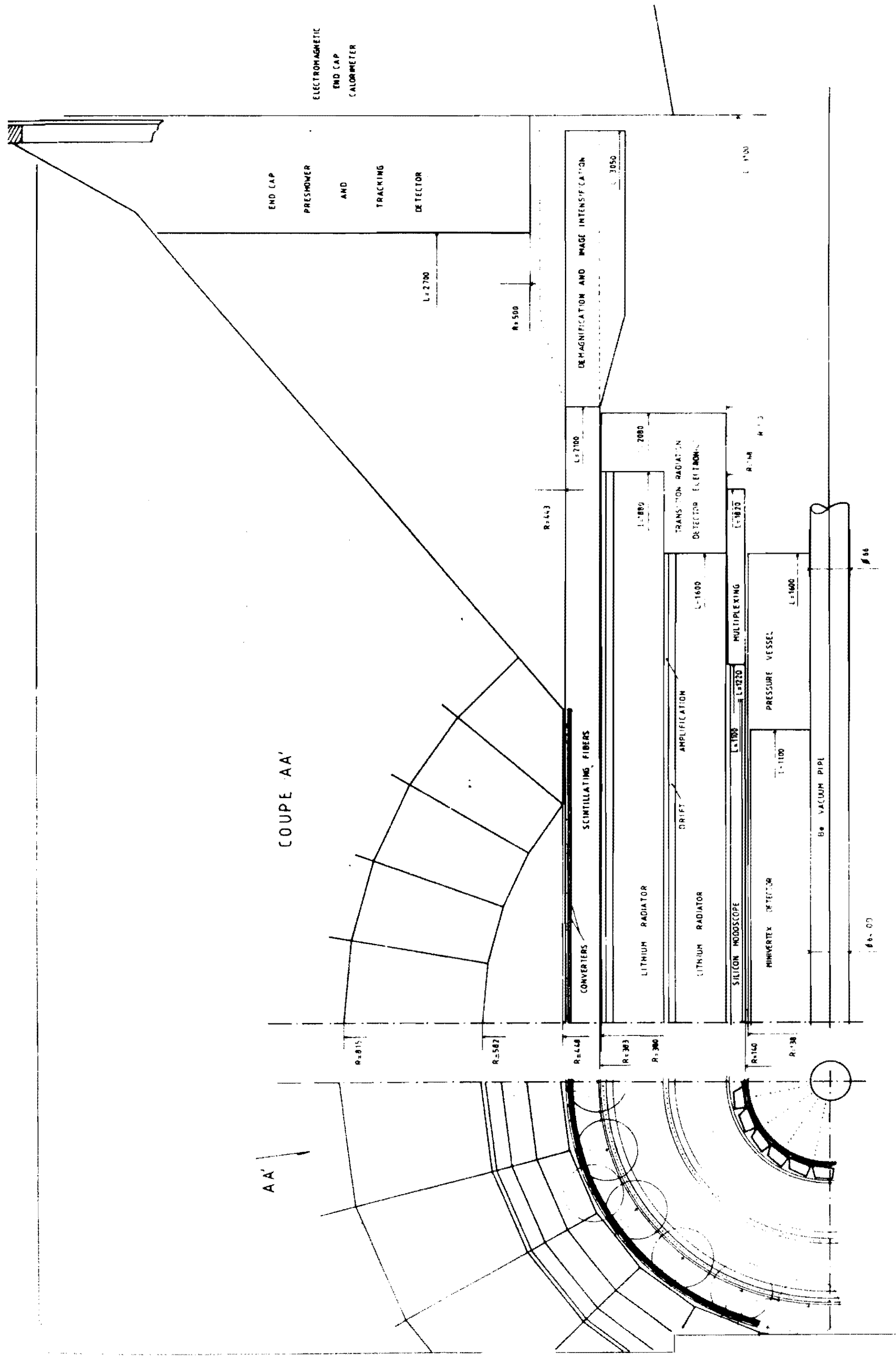
ELECTROMAGNETIC END CAP CALORIMETER
END CAP PRESHOWER AND TRACKING DETECTOR
DEMAGNIFICATION AND IMAGE INTENSIFICATION
TRANSITION RADIATION DETECTOR ELECTRONICS
MULTIPLEXING
PRESSURE VESSEL
COUPE AA'
SCINTILLATING FIBERS
CONVERTERS
LITHIUM RADIATOR
DRIFT
AMPLIFICATION
LITHIUM RADIATOR
SILICON HODOSCOPE
MINIVERTEX DETECTOR
Be VACUUM PIPE
AA'

Fig. 4

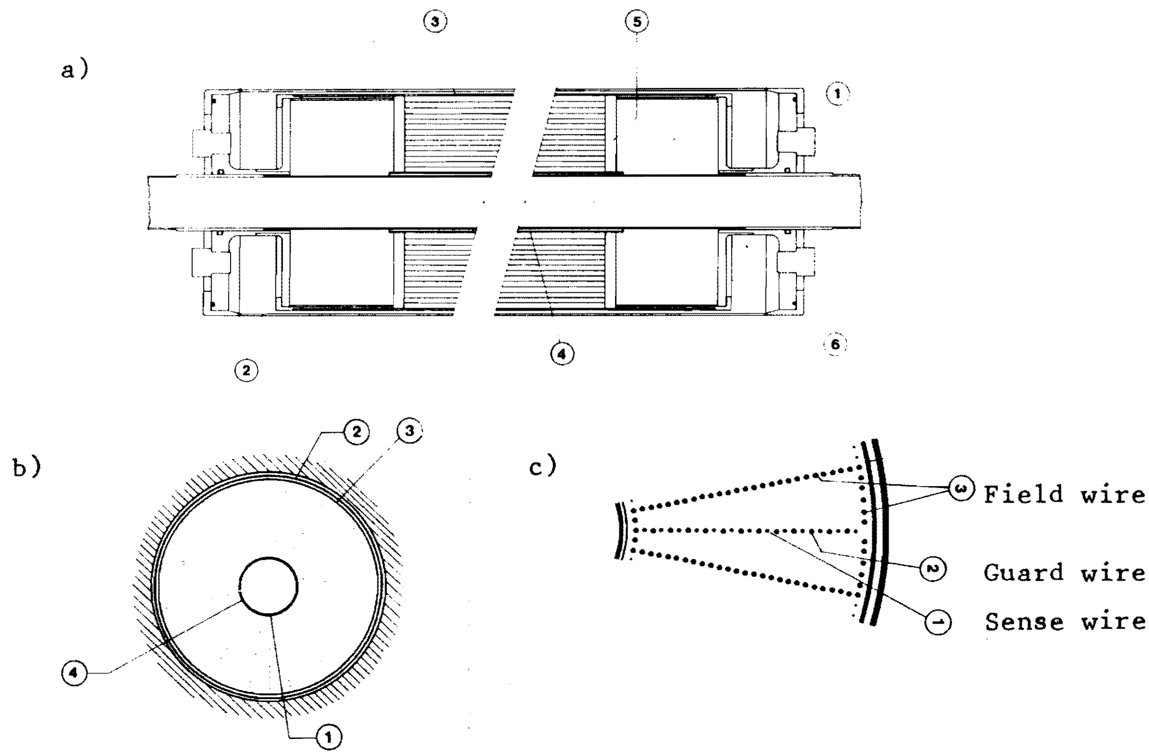
a)
b)
c)
Field wire
Guard wire
Sense wire

Fig. 5

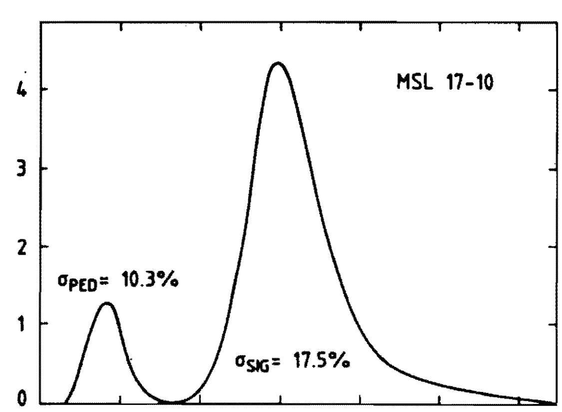
MSL 17-10
σ_{PED}= 10.3%
σ_{SIG}= 17.5%

Fig. 6

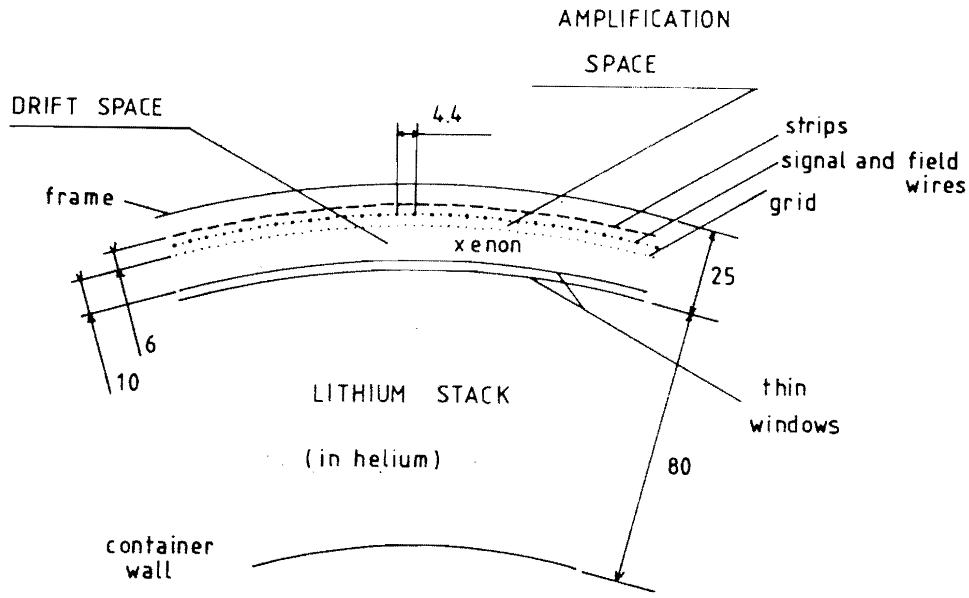

Fig. 7

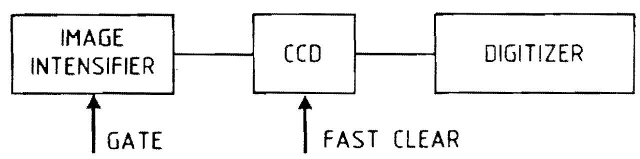

Fig. 8

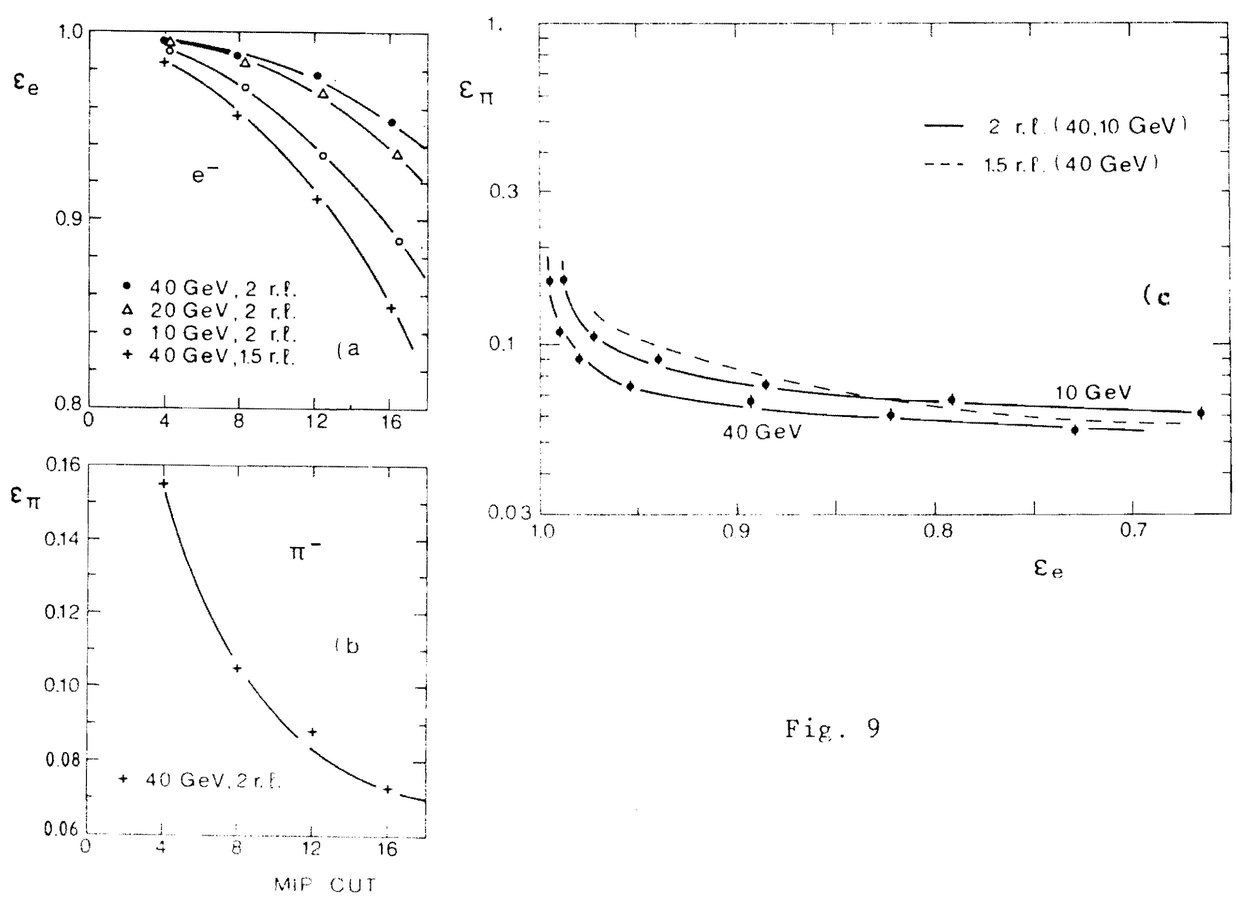

Fig. 9